doi:10.1093/brain/awt278 Brain 2013: 136; 3561–3577 | 3561

BRAIN
A JOURNAL OF NEUROLOGY

Human induced pluripotent stem cell-derived cortical neurons integrate in stroke-injured cortex and improve functional recovery

Daniel Tornero,[1] Somsak Wattananit,[1] Marita Grønning Madsen,[1] Philipp Koch,[2] James Wood,[1] Jemal Tatarishvili,[1] Yutaka Mine,[1] Ruimin Ge,[1] Emanuela Monni,[1] Karthikeyan Devaraju,[1] Robert F. Hevner,[3] Oliver Brüstle,[2] Olle Lindvall[1] and Zaal Kokaia[1]

1 Laboratory of Stem Cells and Restorative Neurology, Lund Stem Cell Centre, University Hospital, SE-221 84 Lund, Sweden
2 Institute of Reconstructive Neurobiology, Life and Brain Centre, University of Bonn and Hertie Foundation, Bonn, Germany
3 Centre for Integrative Brain Research, Seattle Children's Research Institute, Seattle, Washington, USA

Correspondence to: Zaal Kokaia PhD,
Lund Stem Cell Centre,
University Hospital BMC B10,
SE-221 84 Lund,
Sweden
E-mail: zaal.kokaia@med.lu.se

Stem cell-based approaches to restore function after stroke through replacement of dead neurons require the generation of specific neuronal subtypes. Loss of neurons in the cerebral cortex is a major cause of stroke-induced neurological deficits in adult humans. Reprogramming of adult human somatic cells to induced pluripotent stem cells is a novel approach to produce patient-specific cells for autologous transplantation. Whether such cells can be converted to functional cortical neurons that survive and give rise to behavioural recovery after transplantation in the stroke-injured cerebral cortex is not known. We have generated progenitors *in vitro*, expressing specific cortical markers and giving rise to functional neurons, from long-term self-renewing neuroepithelial-like stem cells, produced from adult human fibroblast-derived induced pluripotent stem cells. At 2 months after transplantation into the stroke-damaged rat cortex, the cortically fated cells showed less proliferation and more efficient conversion to mature neurons with morphological and immunohistochemical characteristics of a cortical phenotype and higher axonal projection density as compared with non-fated cells. Pyramidal morphology and localization of the cells expressing the cortex-specific marker TBR1 in a certain layered pattern provided further evidence supporting the cortical phenotype of the fated, grafted cells, and electrophysiological recordings demonstrated their functionality. Both fated and non-fated cell-transplanted groups showed bilateral recovery of the impaired function in the stepping test compared with vehicle-injected animals. The behavioural improvement at this early time point was most likely not due to neuronal replacement and reconstruction of circuitry. At 5 months after stroke in immunocompromised rats, there was no tumour formation and the grafted cells exhibited electrophysiological properties of mature neurons with evidence of integration in host circuitry. Our findings show, for the first time, that human skin-derived induced pluripotent stem cells can be differentiated to cortical neuronal progenitors, which survive, differentiate to functional neurons and improve neurological outcome after intracortical implantation in a rat stroke model.

Keywords: stem cell; stroke; pluripotent; human; cortex

Abbreviations: hCTx = primary cultures of human foetal cortical; PSC = pluripotent stem cells; NES = neuroepithelial-like stem; TTX = tetrodotoxin; WBC = Wnt3a, BMP4 and cyclopamine

Received April 9, 2013. Revised August 12, 2013. Accepted August 13, 2013. Advance Access publication October 21, 2013

Introduction

Ischaemic stroke is a leading cause of death and long-term disability in adult humans. It leads to the loss of brain parenchyma and many types of neurons, astrocytes, oligodendrocytes and endothelial cells. Effective treatments to promote tissue repair and functional recovery after stroke are lacking. Recently, systemic or intracerebral delivery of stem cells has emerged as a promising new therapeutic strategy in stroke. Transplantation of stem cells and their progeny, derived from various sources, has been shown to give rise to improvement in animal models of stroke through several mechanisms including neuronal replacement, modulation of inflammation, neuroprotection and stimulation of angiogenesis (Lindvall and Kokaia, 2011).

Clinical trials with stem cell delivery in stroke patients are ongoing, aiming at improvements through mechanisms other than neuronal replacement (www.clinicaltrials.gov). Although these approaches may provide therapeutic benefit, a long-term goal for stem cell research in stroke should probably be to generate specific neurons for replacement in order to reconstruct injured neural circuitry. In support of this idea, grafted embryonic stem cell-derived neurons can become functional and exhibit some level of synaptic integration in host neural circuitries, suggesting that neuronal replacement in the stroke-damaged brain may contribute to the behavioural improvements (Buhnemann *et al.*, 2006; Hicks *et al.*, 2009; Daadi *et al.*, 2010). Clinical and imaging data showing the distribution of ischaemic cell loss underlying the most severe symptoms in stroke patients indicate that cell replacement approaches should focus on the reconstruction of damaged cortex (Delavaran *et al.*, 2013). This goal will require the generation of cortical neurons from stem cells and their integration following transplantation.

Over recent years, our ability to direct the differentiation of pluripotent stem cells (PSCs) towards specific subtypes of cortical excitatory neurons has vastly improved for mouse cells whereas human cells have lagged behind (Hansen *et al.*, 2011; Ideguchi *et al.*, 2010). Recently, Espuny-Camacho *et al.* (2013) reported that human embryonic stem cells can be differentiated to cortical precursors and integrate after transplantation into the intact neonatal mouse brain. These authors also reported that human induced PSCs, obtained through reprogramming of skin fibroblasts, can generate cortical neuronal precursors *in vitro,* as assessed using gene expression and specific markers (Espuny-Camacho *et al.*, 2013), but no *in vivo* studies were performed. Thus, whether human induced PSC-derived cortical neuronal progenitors can survive transplantation, differentiate to functional, mature cortical neurons and have behavioural effects in the injured adult brain is unknown.

Several recent reports have described that grafts of non-fated human induced PSC-derived neural progenitors, in most cases implanted into the striatum in animals subjected to middle cerebral artery occlusion, can give rise to neurons and improve functional recovery (Chen *et al.*, 2010; Gomi *et al.*, 2012; Jiang *et al.*, 2011; Chang *et al.*, 2012; Polentes *et al.*, 2012). In a previous study (Oki *et al.*, 2012), we used human induced PSC-derived long-term expandable neuroepithelial-like stem (NES) cells, which constitute a stable cell line with capacity to give rise to both mature neurons and glial cells (Falk *et al.*, 2012). After transplantation into the stroke-damaged striatum and cortex, non-fated human induced PSC-derived long-term expandable NES cells stopped proliferation, survived long-term and generated a high proportion of cells with morphological and electrophysiological properties of neurons, providing evidence that human induced PSCs could be used for neuronal replacement in stroke (Oki *et al.*, 2012).

The aims of the present study were 2-fold: first, to generate neuronal progenitors with a cortical phenotype *in vitro* from the human induced PSC-derived long-term expandable NES cells, and second, to transplant these progenitors into the stroke-injured cortex of rats and assess their survival, proliferation, differentiation, morphology and axonal outgrowth, electrophysiological properties, and ability to improve behavioural deficits. We show, for the first time, that intracortically grafted human induced PSC-derived neuronal progenitors, which have been fated towards a cortical phenotype *in vitro*, develop into functional, mature neurons with cortical morphology, integrate into stroke-injured host brain, and promote functional recovery.

Materials and methods

Experimental design

We first evaluated the efficiency of various cortical differentiation protocols on human induced PSC-derived long-term expandable NES cells *in vitro.* Immunohistochemical characterization, PCR confirmation, and electrophysiological analysis were performed at different time points (Supplementary Fig. 1).

For the *in vivo* part of the project, we used Sprague-Dawley and Nude rats, which were subjected to 30 min distal middle cerebral artery occlusion (Supplementary Fig. 1). Three groups of Sprague-Dawley animals were transplanted intracortically with cortically fated or non-fated cells or vehicle 48 h later. Behavioural tests were performed at different time points over 2 months, and animals were then sacrificed for immunohistochemical analysis. Nude rats were transplanted with either non-fated or fated cells 48 h after distal middle cerebral artery occlusion. Behavioural tests were performed over 2 months at the same time points as Sprague-Dawley rats. Twenty to 25 weeks after transplantation, Nude rats were used for electrophysiological recordings (Supplementary Fig. 1). All experimental procedures were approved by the Malmö-Lund Ethical Committee and were conducted in accordance with European Union directive on the subject of animal rights.

Generation of human induced pluripotent stem cell-derived long-term expandable neuroepithelial-like stem cells

The human induced PSC-derived long-term expandable NES cells were produced from dermal fibroblasts as previously described (Falk *et al.*, 2012). Briefly, human fibroblasts were subjected to retroviral transduction with plasmids encoding for the viral glycoprotein VSV-G and the reprogramming factors (Oct4, Sox2, KLF4 and c-MYC) and split into

plates with mouse embryonic fibroblasts. Colonies were then picked and expanded to establish human induced PSC lines. Those lines were induced to differentiate to neural phenotype as previously described (Koch *et al.*, 2009) through an embryoid body-production step. Neural rosettes were generated and carefully picked to isolation of clusters and grown in the presence of 10 ng/ml FGF2, 10 ng/ml EGF (both from R&D systems) and 1 μl/ml B27 (Invitrogen). The human induced PSC-derived long-term expandable NES cell line is routinely cultured and expanded on 0.1 mg/ml poly-L-ornithine and 10 μg/ml laminin (both from Sigma) coated plates into the same media supplemented with FGF, EGF and B27. The human induced PSC-derived long-term expandable NES cells were passaged at a ratio of 1:2 to 1:3 every second to third day using trypsin (Sigma).

Cortical differentiation of human induced pluripotent stem cell-derived long-term expandable neuroepithelial-like stem cells

Growth factors (FGF, EGF) and B27 were omitted and cells were cultured at low density in differentiation defined medium containing Dulbecco's modified Eagle medium/F12 with glutamine (Sigma) and supplemented with N2 (1 ×), non-essential amino acids (0.1 mM), sodium pyruvate (1 mM), bovine serum albumin (500 μg/ml) and 2-mercaptoethanol (0.1 mM), in the presence of BMP4 (10 ng/ml), Wnt3A (10 ng/ml) and cyclopamine (1 μM) for 8 days. Neural progenitors were then dissociated using trypsin and plated on poly-L-ornithine/laminin-coated glass coverslips in Neurobasal/differentiation defined medium (1:1) media supplemented with B27 (1:50 without vitamin A, Invitrogen). For *in vivo* experiments, non-fated cells were grown under the same conditions but without Wnt3A, BMP4 and cyclopamine (WBC).

Quantitative reverse transcription polymerase chain reaction

Quantitative PCR was performed on RNA extracted from cells at Day 32 of differentiation. Non-fated differentiating human iinduced pluripotent stem-derived long-term expandable NES cells were used as controls. Cells were lysed using RLT buffer (Qiagen) directly and stored immediately at −80°C. The RNA extraction from stored samples was performed with RNeasy® micro kit (Qiagen) and 0.5 μg of RNA was used for complementary DNA synthesis with iScript™ Advanced cDNA synthesis kit (Bio-Rad) according to the manufacturer's instructions. Reverse transcription negative control, i.e. complementary DNA synthesis reaction without the reverse transcriptase enzyme, was used to exclude genomic DNA contamination. TaqMan® probes (Life Technologies) were used and quantitative PCR was run in triplicate samples on a iQ5 real time cycler (Bio-Rad). Data were $\log_2$ transformed and fold changes were calculated by the $\Delta\Delta C_T$ method.

Immunohistochemistry

Cells plated on glass coverslips were fixed in 4% paraformaldehyde for 20 min and washed three times in PBS. Permeabilization with 0.025% Triton™ X-100 for 10 min and blocking with 5% normal donkey serum for 45 min were performed. Sprague-Dawley rats were sacrificed 2 months after transplantation and perfused transcardially with 4% paraformaldehyde. Coronal sections (30 μm) were preincubated in blocking solution (5% normal serum and 0.25% Triton™ X-100 in 0.1 M potassium-buffered PBS). Cultures or sections were incubated at +4°C overnight with primary antibodies (Supplementary Table 1) diluted in blocking solution. Fluorophore-conjugated secondary antibodies (Molecular Probes or Jackson Laboratories) were diluted in blocking solutions and applied for 2 h, followed by three rinses. Nuclei were stained with Hoechst (Molecular Probes or Jackson Laboratories) for 10 min followed by three washes and mounting with Dabco®. Images were obtained using epifluorescence and confocal microscopes.

Microscopical analysis and quantification

In vitro quantification was done in three regions of interest from three different coverslips per condition in an epifluorescence/light microscope. Total number of cells in each region of interest was counted using Hoechst staining and CellSens Dimension 2010 software (Olympus, Tokyo, Japan, http://www.olympus.com).

Total number of SC101+ cells in the graft was estimated stereologically using C.A.S.T.-Grid software. Around 500 cells per animal were counted in a predefined fraction of the graft area in an epifluorescence/light microscope. The numbers of cells expressing the other markers was analysed in the same way and results were expressed as percentage of total number of SC101+ cells. For measurements of DCX+ and HuD+ cell numbers and cell morphology, all SC101+ cells in the area adjacent to the core of the grafts were analysed. Colocalization of different markers was in all cases validated in a confocal microscope (Leica, http://www.leica-camera.com).

Projection density in corpus callosum was assessed stereologically using length density estimation with isotropic virtual plane method (newCASTTM, Visiopharm) (Larsen *et al.*, 1998). SC121+ fibres were counted with epifluorescence/light microscope in consecutive sections from +1.60 mm rostral to bregma (beginning of genu of corpus callosum) until 600 μm beyond the cluster of grafted cells.

For pyramidal morphology index determination, the width and the number of dendrites emerging from the cell body were sampled in a circle of 25 μm diameter around the cell body as previously described (Hand *et al.*, 2005). Each pyramidal morphology index was recorded as the width of the largest process divided by the total number of processes that crossed the sampling circle.

Lesion volume was measured using Fox3 staining and C.A.S.T- Grid software. Light microscopic images were first digitalized. The lesion area was calculated by subtracting the non-lesioned (stained) area in the ischaemic hemisphere from the area of the contralateral hemisphere. Lesion volume was estimated by multiplying the areas with section thickness and the distance between the sections.

For evaluating the laminar distribution of TBR1+ cells, grafts were divided in two parts in three representative sections through the central region using a line parallel to the surface of the cortex crossing the centre of the graft. Density of TBR1+ cells in superficial and deep parts of the graft was estimated using C.A.S.T.-Grid software.

To evaluate the rostro-caudal distribution of TBR1+ cells within the grafts, the sections containing grafted cells from each brain were divided into equally sized rostral and caudal groups. The number of TBR1+ cells was counted in each group and results presented as percentage of the total number of TBR1+ cells. When the number of sections was odd, counts in the middle section were distributed equally between the two groups.

Kidney-type glutaminase immunoreactivity was assessed in the grafted non-fated and fated cells. Three images of different regions of the graft in three representative sections from each brain, double-stained

for kidney-type glutaminase and green fluorescent protein (GFP) were acquired. The area of kidney-type glutaminase-immunoreactivity was determined by image analysis using CellSens Dimension 2010 software (Olympus). In each section, areas of immunoreactivity were identified using defined representative ranges of threshold for specific signal. Using these defined parameters, the images of each region were analysed by software, which calculated the total area covered by pixels/specific immunopositive signal. The values corresponding to total fluorescence areas were averaged and expressed as the mean kidney-type glutaminase area per animal.

Electrophysiological recordings

For electrophysiological studies on cultures, cells were grown on coverslips, which were transferred to the recording chamber. Electrophysiological analyses on brain slices were performed as previously described (Oki *et al.*, 2012) except that sagittal sections were used instead of coronal ones.

The recording chamber was constantly perfused with carbogenated artificial CSF (in mM: 119 NaCl, 2.5 KCl, 1.3 $MgSO_4$, 2.5 $CaCl_2$, 26 $NaHCO_3$, 1.25 NaH_2PO_4, and 25 glucose, pH ~7.4) at 34°C. For all measurements of intrinsic properties in cultured cells and in acute slices, recording pipettes were filled with intracellular solution (in mM: 122.5 potassium gluconate, 12.5 KCl, 10 KOH-HEPES, 0.2 KOH-EGTA, 2.0 MgATP, 0.3 Na_2-GTP, and 8.0 NaCl). For measurements of spontaneous and miniature excitatory postsynaptic currents or spontaneous inhibitory postsynaptic currents, the intracellular solution contained (in mM): 117.5 Cs-gluconate, 17.5 CsCl, 8.0 NaCl, 10 CsOH-HEPES, 0.2 CsOH-EGTA, 2 Mg-ATP, 0.3 Na3-GTP, and 5.0 lidocaine N-ethyl bromide (QX-314), or 135.0 CsCl, 10.0 CsOH-HEPES, 0.2 CsOH-EGTA, 2.0 Mg-ATP, 0.3 Na3-GTP, 8.0 NaCl and 5.0 QX-314. Pipette solutions had a pH of 7.2–7.4 and an osmolarity of 285–300 mOsm. Biocytin (0.5%; Sigma-Aldrich) was dissolved in the pipette solution for later identification of recorded cells.

Whole-cell patch-clamp recordings were performed with a HEKA double patch-clamp EPC10 amplifier using PatchMaster for data acquisition. Sodium and potassium currents were evoked by a series of 200 ms long voltage steps (from −70 mV to +40 mV in 10 mV steps) and action potentials were induced by a series of current steps (0–200 pA in 10 pA steps) lasting 500 ms. Voltage-gated sodium and potassium channels were blocked with 1 μM tetrodotoxin (TTX) and 2 mM tetraethylammonium (TEA), respectively. *N*-methyl-D-aspartate (NMDA) and aminomethylphosphonic acid receptors were blocked using 50 μM D-AP5 and 5 μM NBQX, respectively. γ-aminobutyric acid A ($GABA_A$) receptors were blocked using 100 μM picrotoxin. Data were analysed offline with FitMaster.

For electrical stimulation of the intact cortex, the electrode was inserted in the dorsal cortex ~300 μm from the edge of the graft in the caudal direction in a region devoid of green fluorescent protein-positive cells and fibres.

Distal middle cerebral artery occlusion

Focal ischaemic injury in cerebral cortex was induced as described previously (Chen *et al.*, 1986). Briefly, animals were anaesthetized and the temporal bone was exposed. A craniotomy of ~3 mm was made, the dura matter was carefully opened and the cortical branch of middle cerebral artery was ligated permanently by suture. Both common carotid arteries were isolated and temporarily ligated over 30 min. After releasing common carotid arteries, surgical wounds were closed.

Transplantation

Intracerebral transplantation of human induced pluripotent stem-derived long-term expandable NES cells, which had been previously transduced with lentivirus carrying green fluorescent protein, was performed stereotaxically at 48 h after distal middle cerebral artery occlusion in Sprague-Dawley and Nude rats. On the day of surgery, non-fated and fated cells in the seventh day of differentiation were resuspended to a final concentration of 100 000 cells/μl. A volume of 1.5 μl was injected at two sites at the following coordinates (from bregma and brain surface): anterior/posterior: +1.5 mm; medial/lateral: −1.5 mm; dorsal/ventral: −2.0 mm; and anterior/posterior: +0.5 mm; medial/lateral: −1.5 mm; dorsal/ventral: −2.5 mm. Tooth bar was set at −3.3 mm. Sprague-Dawley rats were given subcutaneous injections of 10 mg/kg Cyclosporine A every day during the first month after transplantation and every other day during the second month.

Behavioural tests

In the cylinder test (Andres *et al.*, 2011; Mine *et al.*, 2013), the animal was placed in a glass cylinder (diameter: 20 cm) and its forelimb activity was recorded with a digital video camera. Two perpendicular mirrors were placed behind the cylinder to make the complete surface of the cylinder clearly visible. Forelimb use was defined by the placement of the whole palm on the wall. Such contacts were counted offline using frame-by-frame analysis by an observer blinded to the group identity of the animals up to a total of 20 contacts or over 20 min. The use of each paw was then calculated as a percentage of the total number of touches.

In the stepping test (Olsson *et al.*, 1995), the rats were held by a 'blind' experimenter fixing its hindlimbs with one hand and the forelimb not to be monitored with the other while the unrestrained forepaw was touching a rigid surface. The number of adjusting steps was counted while the rat was slowly moved sideways along the table surface (0.9 m in 5 s), in forehand and backhand directions. The test was repeated twice a day for each forelimb on three consecutive days and the average of the six subtests was calculated.

Statistical analysis

Comparisons were performed using two-way ANOVA, repeated measures ANOVA, and paired or unpaired *t*-test. For studies of correlation, Pearson's correlation coefficient was calculated. Data are presented as mean ± SEM, and differences considered significant at $P < 0.05$.

Results

Cortical progenitors are generated from human induced pluripotent stem cell-derived long-term expandable neuroepithelial-like stem cells

Upon growth factor withdrawal, human induced PSC-derived long-term expandable NES cells differentiate to glial cells and neurons, mostly of GABAergic phenotype (Supplementary Fig. 2) (Falk *et al.*, 2012). To drive the long-term expandable NES cells to an excitatory-glutamatergic neuronal phenotype, we

developed a protocol to derive dorsal-fated cells based on the presence of WBC during the first step of differentiation (priming). Cyclopamine is a sonic hedgehog pathway-inhibitor, which leads to the generation of cortical neurons from mouse embryonic stem cells *in vitro* (Gaspard *et al.*, 2008). We found that the WBC differentiation protocol applied on human induced PSC-derived long-term expandable NES cells gave rise to increased percentage of cells expressing the cortex-specific neuronal marker TBR1 (62.2 ± 2.1%) compared to the cells that were differentiated under the same conditions but without the fating factors (non-fated, 1.5 ± 1.1%; Fig. 1A and B) already after 22 days of differentiation. Other markers like CTIP2 and CDP (characteristic of cells in deeper and superficial layers of the cortex, respectively) were also expressed by the WBC-primed cells (fated) at 30 days of differentiation (2.1 ± 1.0% and 5.7 ± 2.2% respectively; Fig. 1C–E), but were not detectable in non-fated cells. We did not observe an increment in the number of mature neurons (MAP2+) in the cells subjected to WBC priming, probably because the long-term expandable NES cells already formed maximum number of neurons in the non-fated condition (Falk *et al.*, 2012). This number is 74.8 ± 1.7 % after 22 days of differentiation and decreases to 49.6 ± 2.1 % at 30–35 days. We observed that cells continued to proliferate at both time points, and found a gradual increase of the number of GFAP+ cells after 20 days, amounting to ~30% of the total number of cells after 35 days. There was also some minor neuronal death during differentiation. Thus, the lower percentage of neurons at 30–35 as compared with 22 days of differentiation was most likely due to a combination of neuronal death and delayed appearance and higher proportion of mature glial cells, consistent with previous data using mouse embryonic stem cells (Gaspard *et al.*, 2009). At the later time point, very few cells (<0.1%) expressed the marker DARPP32, characteristic of medium-spiny striatal neurons (Fig. 1H and I), whereas the vast majority of neurons (~80% of the β-III tubulin and/or MAP2+ cells) expressed the glutamatergic neuron-specific protein VGlut1 (Fig. 1F).

Analysis of messenger RNA levels using quantitative PCR at Day 32 of differentiation confirmed an increase of specific cortical markers such as *TBR1* and *CTIP2* in the fated cells compared with non-fated ones (Fig. 1G). We did not detect an increase of the glutamatergic marker *V-GLUT1*, suggesting that the switch to a cortical fate occurs among the glutamatergic phenotype of cells. Interestingly, the presence of cyclopamine attenuated the *CTIP2* messenger RNA levels (Fig. 1G). This finding is probably because of the presence of *CTIP2* not only in layer V of the cortex but also in the striatum, reflecting the dorsalization of the cells induced by the WBC protocol.

At the latest analysed time point (Day 35), synapsin I- and glial specific marker GFAP+ cells were observed among the fated cells (Fig. 1J–M). In agreement, it has been shown by other *in vitro* studies on mouse embryonic stem cells and human embryonic stem cells and induced PSCs (Gaspard *et al.*, 2008; Shi *et al.*, 2012) that GFAP+ cells appear at later time points whereas the percentage of MAP2+ and β-III tubulin+ cells decreases, thus recapitulating *in vivo* corticogenesis.

Cortically fated cells show electrophysiological properties of functional neurons

Whole-cell patch-clamp recordings from 26 non-fated and 31 fated cells were performed at 15–22 days of differentiation (early time point) or 30–34 days of differentiation (late time point). Recordings from primary cultures of human foetal cortical (hCTx) neurons ($n = 10$) at 22–23 days *in vitro* were performed for comparison (Supplementary material). The properties of the non-fated and fated cells, which were able to generate at least one action potential, and those of the hCTx cells were measured (Table 1).

Depolarizing current injection induced action potentials in 50–74% of the non-fated and fated cells at the early time point (Table 2, Supplementary Fig. 3 and 4). At the late time point, both non-fated and fated cells were able to generate multiple action potentials (Fig. 2A, Table 2) as observed for hCTx cells (Table 2, Supplementary Fig. 5). The characteristics of the action potentials recorded from non-fated and fated cells at the late time point, and to some extent also at the early time point, were similar to those observed for hCTx cells (Table 2).

In a subset of recordings, the sodium channel blocker TTX was applied. In all of these recordings, TTX abolished the action potential generation in hCTx as well as in non-fated and fated cells both at the early and late time point (Fig. 2B and Supplementary Fig. 3, 4 and 5). Voltage clamp recordings revealed the presence of a TTX-sensitive sodium current (fast inward current, Fig. 2C and D and Supplementary Fig. 3, 4 and 5) and a TEA-sensitive potassium current (sustained outward current; Supplementary Fig. 3, 4 and 5). The profile of curves obtained by plotting the current amplitude against the voltage appeared similar for both sodium and potassium currents in the non-fated, fated and hCTx cells (Supplementary Fig. 3, 4 and 5).

To confirm the neuronal identity of the recorded biocytin-labelled cells, we used staining for the mature neuronal marker MAP2 and the cortex-specific marker TBR1 (Fig. 2E and F). Most (16 of 18) of the biocytin-labelled cells were MAP2+ at the late time point, and seven of the MAP2+ cells were TBR1+.

Cortically fated cells are fewer and proliferate less than non-fated cells two months after transplantation in stroke-damaged cortex

Rats subjected to 30 min of distal middle cerebral artery occlusion received intracortical injections of non-fated or fated cells or vehicle 48 h later. After 2 months, animals showed lesions that were homogeneous in size and restricted to the cortex in all three groups (Supplementary Fig. 6A) with sparing of subcortical structures. Somatosensory cortex and some areas of the motor cortex were affected. In the rostro-caudal axis, the lesion included both frontal and parietal cortical areas with volume ~70 mm^3 (Supplementary Fig. 6A and B).

Using the human specific nuclear marker SC101 and stereological counting, we found that the number of cells in the grafts was almost

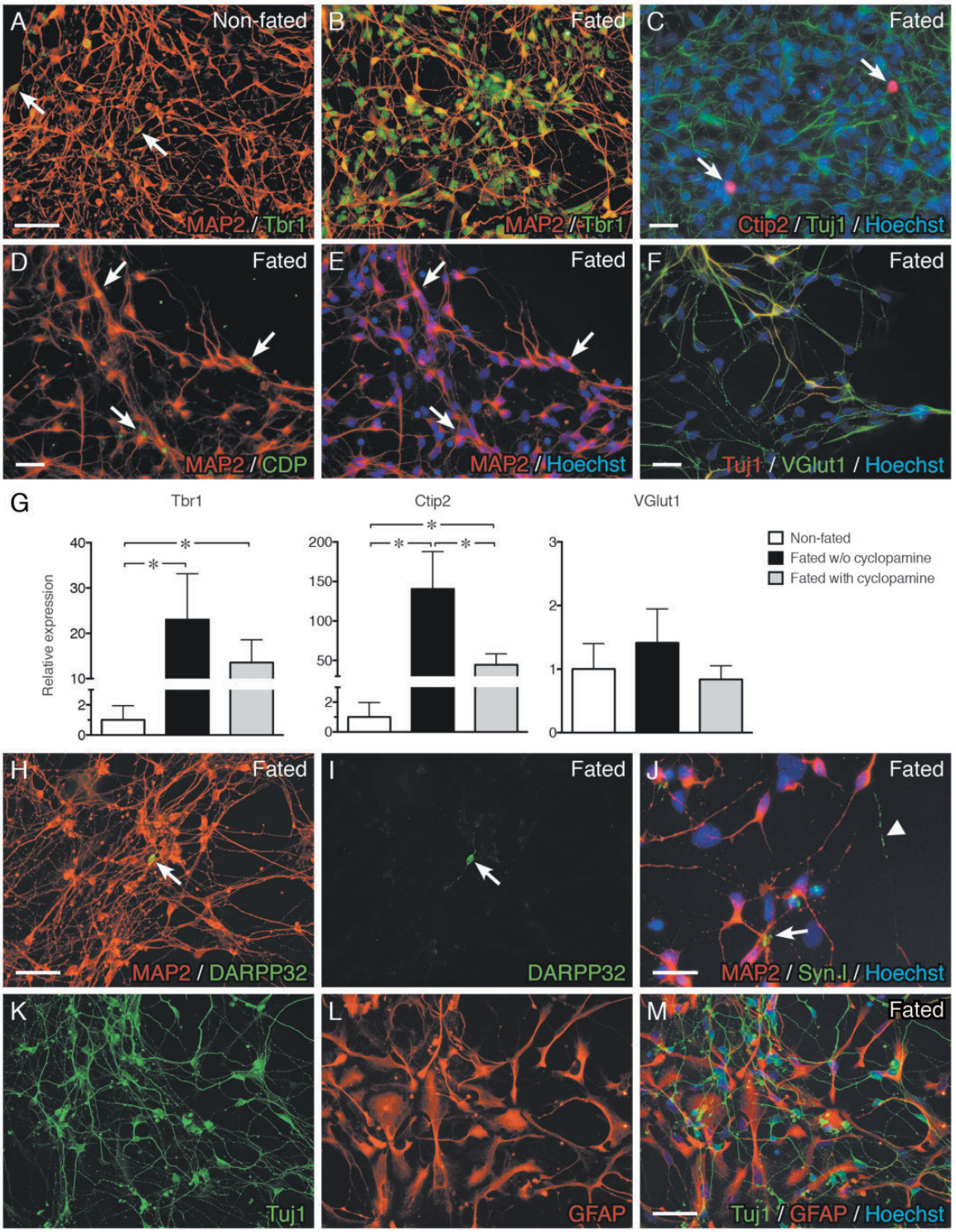

Figure 1 Cells with phenotype of cortical neurons can be generated from human induced PSC-derived long-term expandable NES cells *in vitro*. (**A** and **B**) Photomicrographs showing that differentiation of human induced PSC-derived long-term expandable NES cells for 22 days generates MAP2 + cells under non-fated (**A**) and fated conditions (**B**). Note the increased number of TBR1 + cells in cultures treated with WBC, only a few depicted by arrows in non-fated. (**C–F**) Photomicrographs of fated cells at 30 days of differentiation immunoreactive for layer V cortical marker CTIP2 (**C**; arrows), for the superficial cortical layers CDP (**D** and **E**; arrows) and for glutamatergic neuronal protein VGLUT1 (**F**; green colour). (**G**) Quantitative PCR analysis of gene expression (TBR1, CTIP2 and VGLUT1) in fated cells fated with or without cyclopamine, and non-fated cells after 32 days of differentiation. Means ± SEM. $*P < 0.05$, one-way ANOVA test. (**H** and **I**) Photomicrographs for the striatal neuronal marker DARPP32 under fated condition (arrow depicts single DARPP32 + cell). (**J**) Photomicrographs of fated cells showing synapsin I immunoreactivity in neurites (arrowhead) and cell bodies (arrow) after 35 days of differentiation. (**K–M**) Photomicrographs showing Tuj1 (neuronal maker) and GFAP (astrocyte marker) in **K** and **L**, respectively, and as merged image (**M**) in fated cultures. Scale bars: **A**, **B** **H**, **I**, **K**, **L** and **M** = 100 μm; in **C**, **D**, **E**, **F** and **J** = 50 μm.

Table 1 Electrophysiological properties of cultured non-fated, fated, and hCTx cells generating one or more action potentials upon current injections

	Non-fated		Fated		hCTx
Time point	Early	Late	Early	Late	
n	8	7	14	6	10
V_{rest} (mV)	−46.3 ± 2.4	−32.4 ± 4.2*	−40.7 ± 2.5*	−34.9 ± 3.5*	−54.8 ± 3.2
R_{input} (MΩ)	917 ± 134	1069 ± 191	1479 ± 200*	1254 ± 181	704 ± 70
C (pF)	9.7 ± 3.2	7.8 ± 1.0	17.5 ± 5.3	8.9 ± 1.3	13.6 ± 2.5

V_{rest} = resting membrane potential; R_{input} = input resistance; C = capacitance.
*significant different from hCTx (V_M: ANOVA $P < 0.0001$, Tukey's multiple comparison test $P < 0.001$ for non-fated and $P < 0.01$ for fated; R_{input}: ANOVA $P = 0.0097$, Dunn's multiple comparison test $P < 0.01$).

Table 2 Action potential characteristics for cultured non-fated, fated and hCTx cells

	Non-fated		Fated		hCTx
Time point	Early	Late	Early	Late	
% cells with AP (cells with AP/total)	50 (8/16)	70 (7/10)	74 (14/19)	50 (6/12)	100 (10/10)
Number of APs	8.0 ± 2.1	4.7 ± 1.9	2.8 ± 0.7*	7.3 ± 2.9	9.9 ± 1.3
AP threshold (mV)$	−27.7 ± 1.3	−25.8 ± 1.9	−24.5 ± 1.0	−27.1 ± 1.2	−26.5 ± 1.2
AP amplitude (mV)$	49.2 ± 6.0	41.6 ± 7.2	57.8 ± 3.4#	34.1 ± 3.5	51.3 ± 3.4
AP half-height width (ms)$	3.2 ± 0.5	2.4 ± 0.5	3.0 ± 0.3	3.6 ± 1.0*	1.5 ± 0.1
AHP amplitude (mV)$	7.6 ± 1.7*	12.0 ± 3.4	7.7 ± 1.5*	17.6 ± 6.4	20.6 ± 1.2

AP = action potential; AHP = after hyperpolarization.
$Analysis based on the first action potential induced by current injection.
*Significant different from hCTx (number of action potentials: ANOVA $P = 0.0084$, Bonferroni's multiple comparison test $P < 0.01$; action potential half-height width: ANOVA $P = 0.0298$, Tukey's multiple comparison test $P < 0.05$; AHP amplitude: ANOVA $P = 0.0005$, Tukey's multiple comparison test $P < 0.01$ for non-fated and $P < 0.001$ for fated).
#Significantly different from fated cells at the late time point (ANOVA $P = 0.0111$, Tukey's multiple comparison test $P < 0.01$).

2-fold higher in the non-fated compared to the fated group ($1.58 \pm 0.33 \times 10^6$ and $0.81 \pm 0.16 \times 10^6$, respectively; Fig. 3A). In both groups, grafted cells had migrated from the injection site towards the ischaemic lesion, refilling part of the stroke cavity (Fig. 3C and E).

In order to explore whether the different number of cells in the grafts in the non-fated and fated groups could be due to differences in proliferation, we analysed the expression of Ki67 in cells positive to SC101. In support of this idea, stereological counting demonstrated a significantly higher proliferation rate for non-fated as compared to fated cells (30.1 ± 6.3% and 10.4 ± 3.0%, respectively; Fig. 3B, D and F). To exclude the possibility that increased apoptotic rate had caused the reduced number of cells in the fated grafts as compared to the number of cells in the grafts of non-fated cells, we performed terminal deoxynucleotidyl transferase dUTP nick end labeling (TUNEL) staining in both groups. Stereological estimation of apoptotic cells revealed a rate of 0.46 ± 0.11% for the non-fated group and 0.35 ± 0.08% for the fated group, with no significant difference between them.

Transplantation of cortically fated cells into stroke-damaged cortex improves recovery of sensorimotor deficits

Sensorimotor function was evaluated using the cylinder and stepping tests at 1, 4 and 8 weeks after the ischaemic insult in rats injected intracortically with vehicle or non-fated or fated cells. In the cylinder test, the percentage of touches with each forelimb reflects its spontaneous use. One week after stroke, animals in all three groups showed reduced use of the left forelimb but no impairment was detected 7 weeks later (Fig. 4A). The stepping test provides a direct measure of the sensorimotor deficit underlying limb akinesia. The cortical lesion caused a significant bilateral reduction of forelimb adjusting steps in the forehand direction (Fig. 4B and C), reaching maximum at 1 week after stroke in the contralateral forelimb (Fig. 4B), whereas there was a further decline at 4 and 8 weeks in the ipsilateral forelimb (Fig. 4C). No recovery was observed in the vehicle-injected group by 8 weeks. When the same data were analysed together with groups that received transplantation of fated or non-fated cells we detected an improved performance in adjusting steps of both forelimbs in the forehand direction compared with vehicle-injected animals at 8 weeks (Fig. 4D and E). We observed no differences in this test between animals grafted with fated or non-fated cells. Compared with the forehand direction, the impairment after stroke was smaller in the backhand direction and it was not influenced by the grafts (data not shown).

Fated cells differentiate to neurons with cortical phenotype after transplantation in stroke-damaged cortex

To characterize the morphological properties of the grafted cells and their progeny, we used neuronal markers in combination with

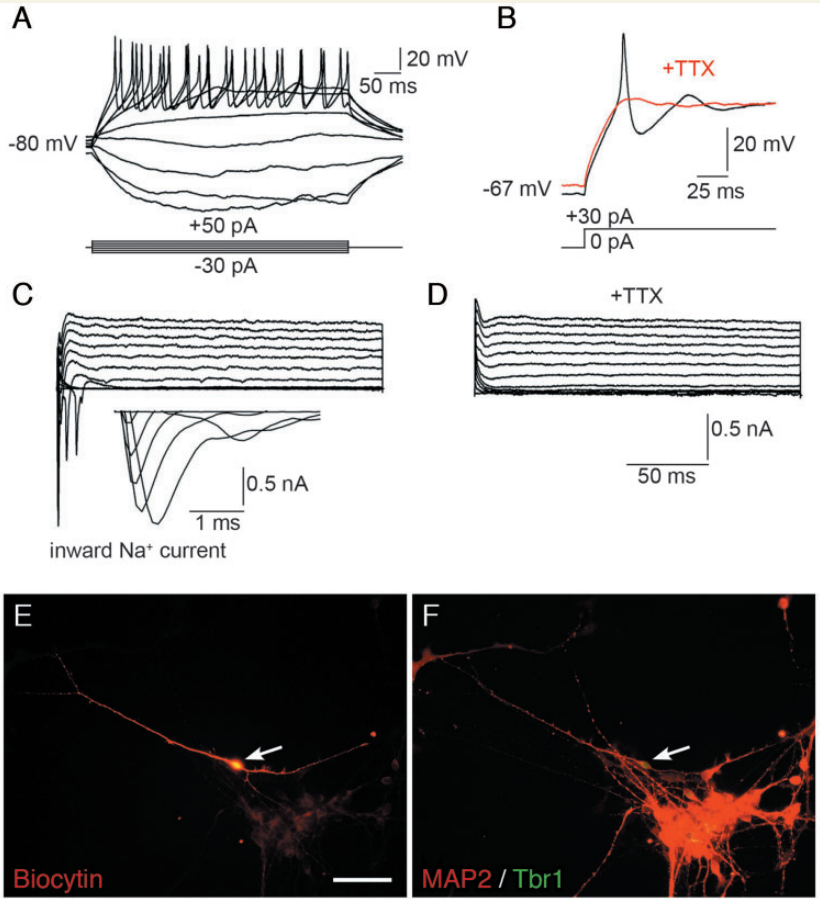

Figure 2 Cortically fated cells exhibit electrophysiological properties of neurons after 30–35 days of differentiation *in vitro*. (**A**) Representative voltage traces from a cortically fated cell. (**B**) A train of action potentials is generated upon current injection (10 pA current steps from −30 to +50 pA). Action potentials are blocked in the presence of 1 μM TTX. (**C** and **D**) Representative traces of the fast inward Na+ current (**C**), which is blocked by 1 μM TTX and the remaining sustained outward K+ current (**D**), elicited by voltage steps from −70 mV to +40 mV in 10 mV increments. (**E** and **F**) Photomicrographs of recorded biocytin-labelled cell (**E**; arrow) stained for MAP2 and TBR1 (**F**). Scale bar = 100 μm.

human-specific and green fluorescent protein antibodies. Due to high number and density of cell bodies and fibres, it was not possible to carry out a quantitative analysis in the core of the graft in sections immunostained with cytoplasmic antibodies like DCX and HuD. Therefore, detailed assessment of the neuronal phenotype was performed on cells located outside the graft core as previously described (Darsalia *et al.*, 2007). At 2 months after transplantation, most cells in the graft were stained for DCX (72.2 ± 1.8% for non-fated and 77.1 ± 4.3% for fated cells; Fig. 5A and B), which is expressed by proliferating cells, committed to a neuronal phenotype, and also by immature neurons. The marker HuD, which is specific for post-mitotic neurons including immature and mature but not proliferating cells, was also found in the majority of grafted cells (65.0 ± 3.1% for non-fated and 77.4 ± 3.9% for fated cells; Fig 5A, and C–E), the percentage being significantly higher in animals transplanted with fated as compared to non-fated cells. A substantial number of grafted cells also expressed the mature neuron-specific marker Fox3 (7.1 ± 0.8% for non-fated and 13.7 ± 2.6% for fated cells; Fig. 5A, and F–H), with significantly higher proportion in the fated cell transplanted group. Finally, a small number of fated and non-fated cells (< 1%) expressed the glial-specific marker GFAP at this time-point.

We then analysed the expression and distribution of cortical markers like TBR1, which is mainly present in cortical layers 5 and 6 of adult brain, SATB2, present in cortical neurons that extend axons across the corpus callosum, and CDP, which is a specific marker of superficial layers of the cortex (layers 1, 2 and 3), in the grafts. The nuclear location of these markers allowed for evaluation also in the core of the graft. At 2 months after transplantation, we detected a considerable number of TBR1+ cells with significantly higher percentage in the grafts of fated cells (2.5 ± 0.3% versus 1.4 ± 0.2% in grafts of non-fated; Fig. 6A) showing in most of the cases pyramidal morphology characteristic of cortical neurons (Fig. 6B–D). Other cortical markers like CDP or SATB2 were detected only in very few cells in both grafts, probably due to the later appearance of these markers during neuronal development (see example of CDP+ cells in Supplementary Fig. 7). Considering the preferential localization of TBR1+ cells in the deeper cortical layers in the intact adult brain (Shoemaker and

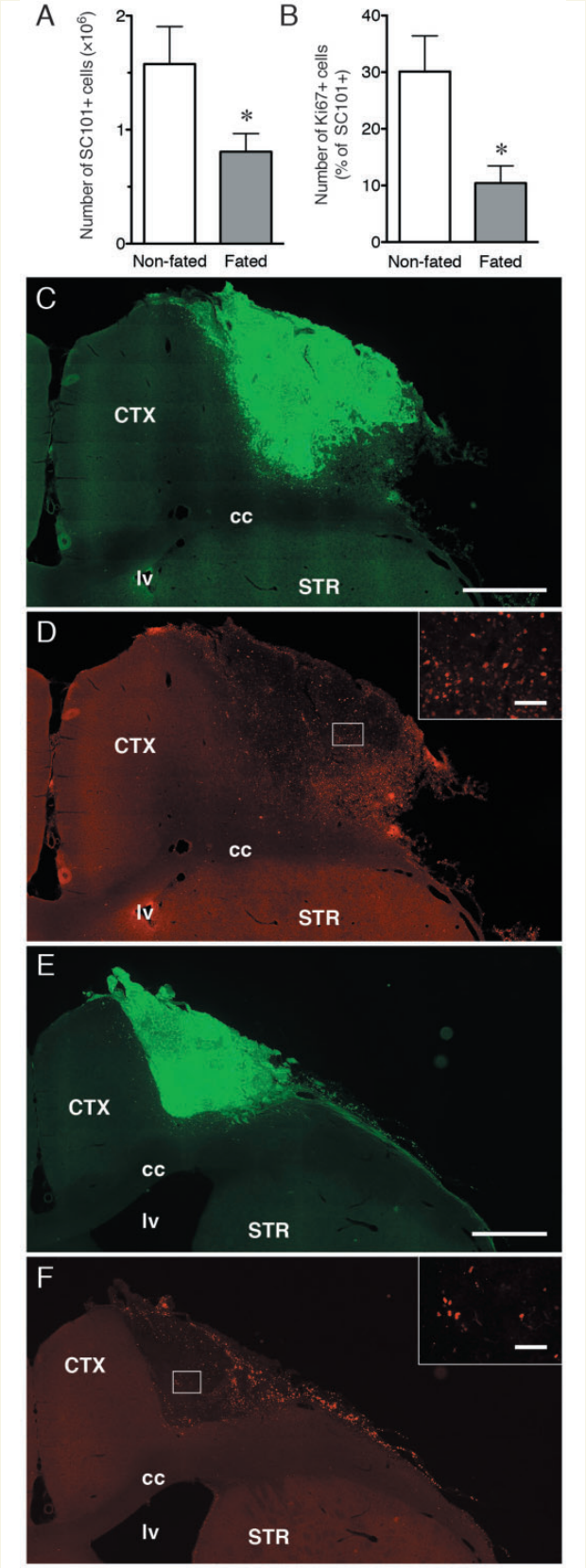

Figure 3 Cortically fated cells are fewer and proliferate less than non-fated cells after transplantation. (**A** and **B**) Stereological quantification of total number of SC101+ cells (**A**) and percentage of proliferating Ki67+ cells (**B**) in the grafts 2 months after implantation. Means ± SEM. $*P < 0.05$, Student's unpaired *t*-test. (**C–F**) Photomicrographs of two representative animals with grafts of non-fated (**C** and **D**) and fated (**E** and **F**) cells stained for GFP (**C** and **E**) and Ki67 (**D** and **F**). Insets in **D** and **F** show higher magnification of the white square. Scale bars: **C–F** = 1 mm ; insets = 200 µm. cc = corpus callosum; lv = lateral ventricle; CTX = cortex; STR = striatum.

Arlotta, 2010), we decided to analyse the distribution of these cells within the grafts in all animals from both groups. Interestingly, we found a 3-fold higher density of TBR1+ cells in the deeper layers of the grafts containing fated compared to those with non-fated cells (Fig. 6E–G). This finding suggests that fated cells implanted into the stroke-damaged brain reconstitute more closely than non-fated cells the normal distribution pattern of TBR1 expression across the cortex structure. We also found a preferential distribution of TBR1+ cells in the rostral part of the graft in animals transplanted with fated cells. In contrast, TBR1+ cells were distributed equally through the rostro-caudal axis in animals with grafts of non-fated cells (Fig. 6H).

To provide further evidence for the cortical phenotype of the fated grafted cells, we quantified the immunoreactivity for the glutamatergic neuron-specific marker kidney-type glutaminase. Computer-based, unbiased analysis of the sections revealed that the area of kidney-type glutaminase immunoreactivity in the grafts was significantly larger in the fated as compared to the non-fated group (Fig. 6I–O).

Fated cells generate higher projection density and exhibit more cortical morphological properties than non-fated cells after transplantation in stroke-damaged cortex

Using the human-specific cytoplasmic marker SC121 combined with green fluorescent protein immunostaining to identify the grafted cells and their projections, we observed fibres migrating through the ipsilateral cortex adjacent to the graft, many crossing the corpus callosum, with some reaching the contralateral hemisphere, and a few fibres migrating subcortically towards the internal capsule.

Quantification of these graft-derived fibres in the corpus callosum showed a several-fold higher density in animals transplanted with fated cells (157.3 ± 91.9 fibres/mm^2 for non-fated and 652.2 ± 176.7 fibres/mm^2 for fated cells, Fig. 7A–C). Interestingly, we found a linear correlation between the percentage of TBR1+ cells in the graft and the projection density in the corpus callosum ($P = 0.015$, $R^2 = 0.38$, Pearson test).

Cortical excitatory neurons are known to exhibit a typical pyramidal morphology, characterized by a polarized outgrowth of one major dendrite, whereas the vast majority of GABAergic interneurons are unpolarized or bipolar. Using a pyramidal morphology index to objectively distinguish the dentritic morphology (Hand *et al.*, 2005), we compared the shape of the neurons generated

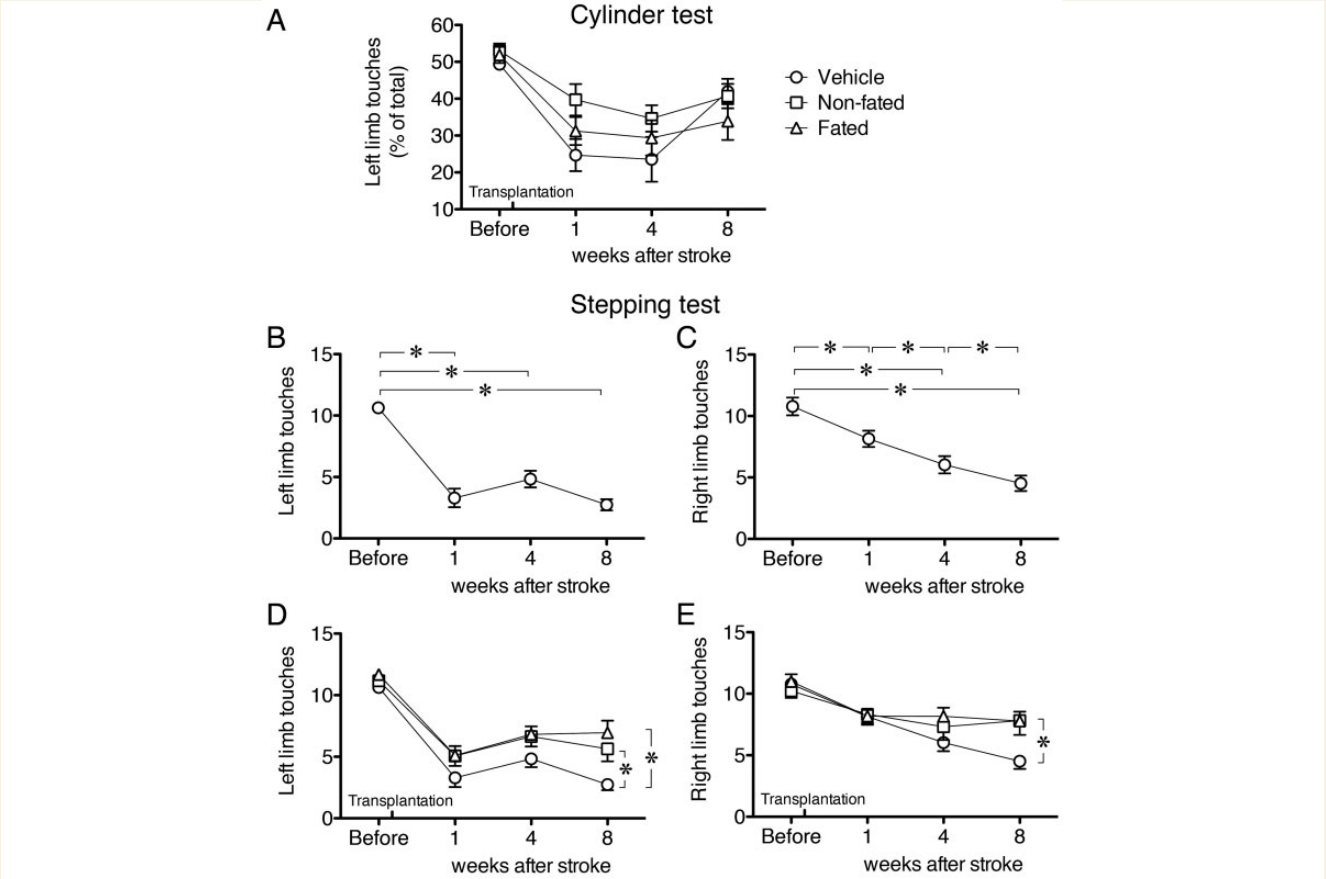

Figure 4 Transplantation of cortically fated and non-fated cells into cortex of stroke-damaged rats induces behavioural improvement. (**A–E**) Comparisons between vehicle-injected ($n = 14$), and non-fated ($n = 12$) and fated ($n = 14$) cell-transplanted rats subjected to right side distal middle cerebral artery occlusion in performance in cylinder (**A**) and stepping (**B–E**) tests. Performance for impaired limb in the cylinder test was calculated as percentage of total number of touches. Performance in the stepping test is presented as number of touches with left (**B** and **D**) and right (**C** and **E**) forelimbs in forehand direction. (**B** and **C**) Time-course of the performance after stroke in vehicle-injected animals. Means ± SEM. $*P < 0.05$, one-way ANOVA. (**D** and **E**) Comparison of performance in the three groups showing a significant bilateral improvement at 8 weeks in animals receiving both fated and non-fated cells. Means ± SEM. $*P < 0.05$, two-way ANOVA.

in each condition in the area adjacent to the core of the graft. Interestingly, in the grafts of fated cells we observed a markedly higher percentage of neurons with pyramidal morphology and lower percentage with bipolar morphology as compared to grafts of non-fated cells (Fig. 7D–H). The analysis resulted in a pyramidal morphology index of 2.3 ± 0.1 for non-fated and 3.0 ± 0.2 for fated grafts ($P = 0.02$).

Cortically fated cells show electrophysiological properties of functional neurons five months after transplantation in stroke-damaged cortex

We wanted to determine whether the fated and non-fated cells could differentiate to functional neurons also *in vivo*. To avoid immunosuppressive treatment and allow for long-term survival, we used Nude rats, which were subjected to 30 min of distal middle cerebral artery occlusion and received intracortical injections of either non-fated or fated cells 48 h thereafter.

Twenty to 25 weeks later, whole-cell patch-clamp recordings were performed in acute brain slices (48 fated and 20 non-fated cells from five rats in each group). We found that 21% and 35% of the fated and non-fated cells, respectively, showed functional properties of mature neurons and were able to fire action potentials induced either by depolarizing current injection or spontaneously (Fig. 8A and B and Tables 3 and 4).

Synaptic transmission, determined by the detection of postsynaptic currents, was observed in the majority of recorded cells (Fig. 8C). Spontaneous or miniature glutamatergic spontaneous excitatory postsynaptic currents were detected in the presence of $GABA_A$ receptor antagonist picrotoxin and could be inhibited in the presence of NMDA and aminomethylphosphonic acid antagonists D-AP5 and NBQX, respectively (Fig. 8D and E and Supplementary Fig. 8B). Similar to our previous findings at 5 months after transplantation of human induced PSC-derived

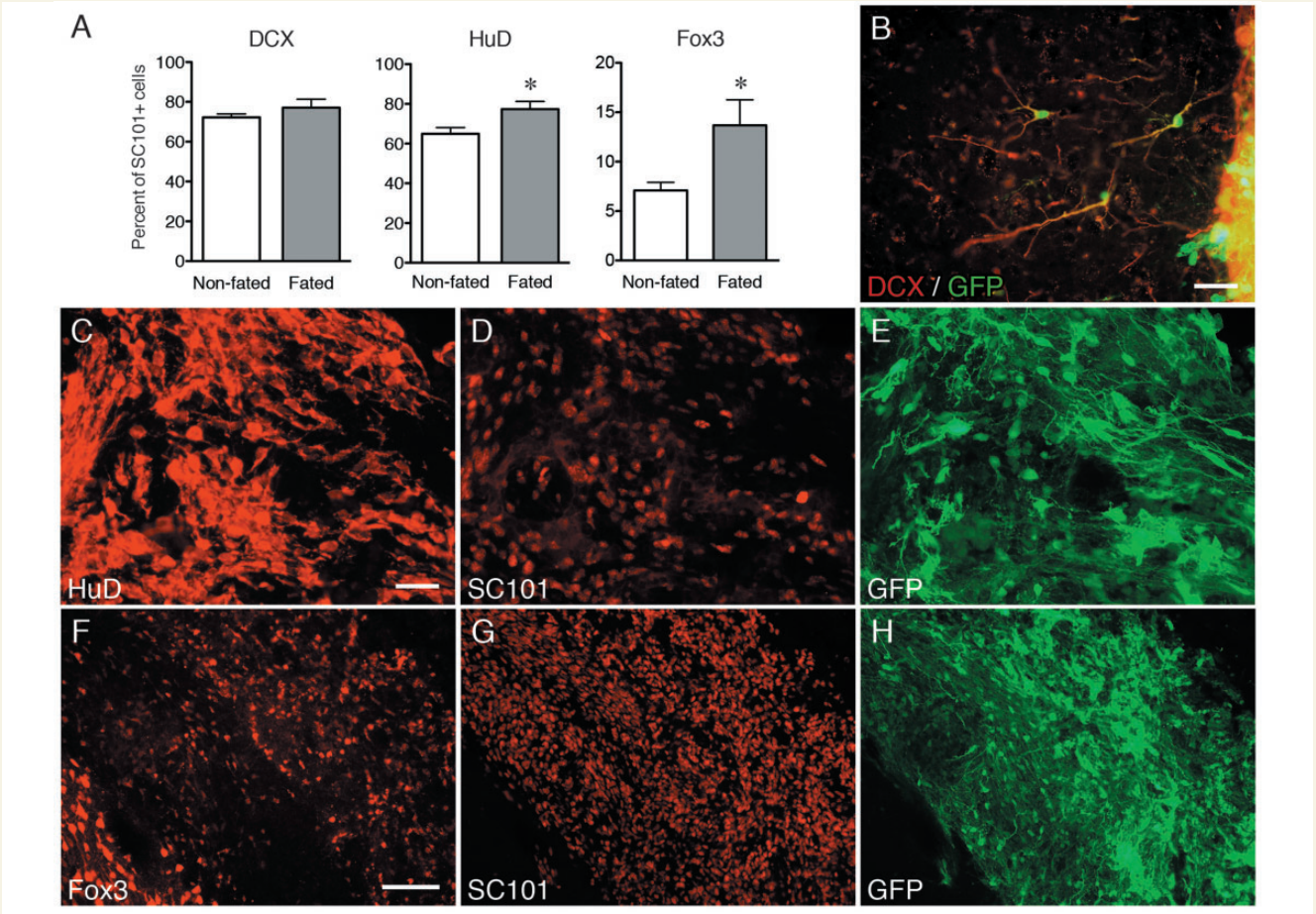

Figure 5 Cortically fated cells differentiate to neurons after transplantation in stroke-damaged cortex. (**A**) Quantification of transplanted non-fated and fated human cells immunoreactive for DCX and HuD in the periphery of the graft, and Fox3 in the whole graft expressed as percentage of SC101+ cells. Means ± SEM. $*P < 0.05$, Student's unpaired *t*-test. (**B–H**) Photomicrographs of representative images of transplanted fated cells stained with antibodies against DCX (**B**), HuD (**C**) and Fox3 (**F**) with reference staining for SC101 (**D** and **G**) and GFP (**B**, **E** and **H**). Scale bars: **B**, **C** and **E** = 50 μm; **F**, **G** and **H** = 100 μm.

long-term expandable NES cells into the unlesioned rat cortex (Oki *et al.*, 2012), we did not detect spontaneous induced PSCs in the grafted fated cells. Following electrical stimulation of the intact cortex adjacent to the transplant of fated cells, we recorded a monosynaptic evoked response (Fig. 8F). This finding suggests that host circuitry had developed functional synapses with the grafted cells, or that grafted cells extended processes to the location of the stimulating electrode. Taken together, our results demonstrate that fated (as well as non-fated) human induced PSC-derived long-term expandable NES cells become mature, functional neurons after transplantation into the stroke-injured cerebral cortex.

Discussion

We present here the first experimental evidence that human skin-derived induced PSCs can be differentiated to a cortical neuronal phenotype and partly reconstitute injured cortex and improve neurological outcome after intracortical transplantation in a rat stroke model. The human induced PSC-derived long-term expandable NES cells were efficiently differentiated to a neuronal phenotype *in vitro* without the addition of neural inducers like noggin, SB43152 or dorsomorphin as previously described (Kim *et al.*, 2010; Shi *et al.*, 2012). We performed the priming step to generate cortical neuronal precursors in the presence of BMP4 and Wnt3a, to promote appropriate differentiation to mature neurons (Andersson *et al.*, 2011; Hebert *et al.*, 2002; Kuwabara *et al.*, 2009; Shimogori *et al.*, 2004), and cyclopamine to inhibit possible Shh activation and ensure the dorsal phenotype (Gaspard *et al.*, 2008; Li *et al.*, 2009). However, recent data have indicated that cyclopamine may not be necessary for the induction of cortical identity in human stem cells (Espuny-Camacho *et al.*, 2013). Immunohistochemical characterization of our fated cells at different time points confirmed the expression of markers specific for mature cortical neurons and glial cells with a pattern similar to that observed in other *in vitro* models using human induced PSCs (Mariani *et al.*, 2012). The fated cells also showed electrophysiological properties and quantitative PCR profile resembling those of neurons in human foetal primary cortical cultures, confirming their

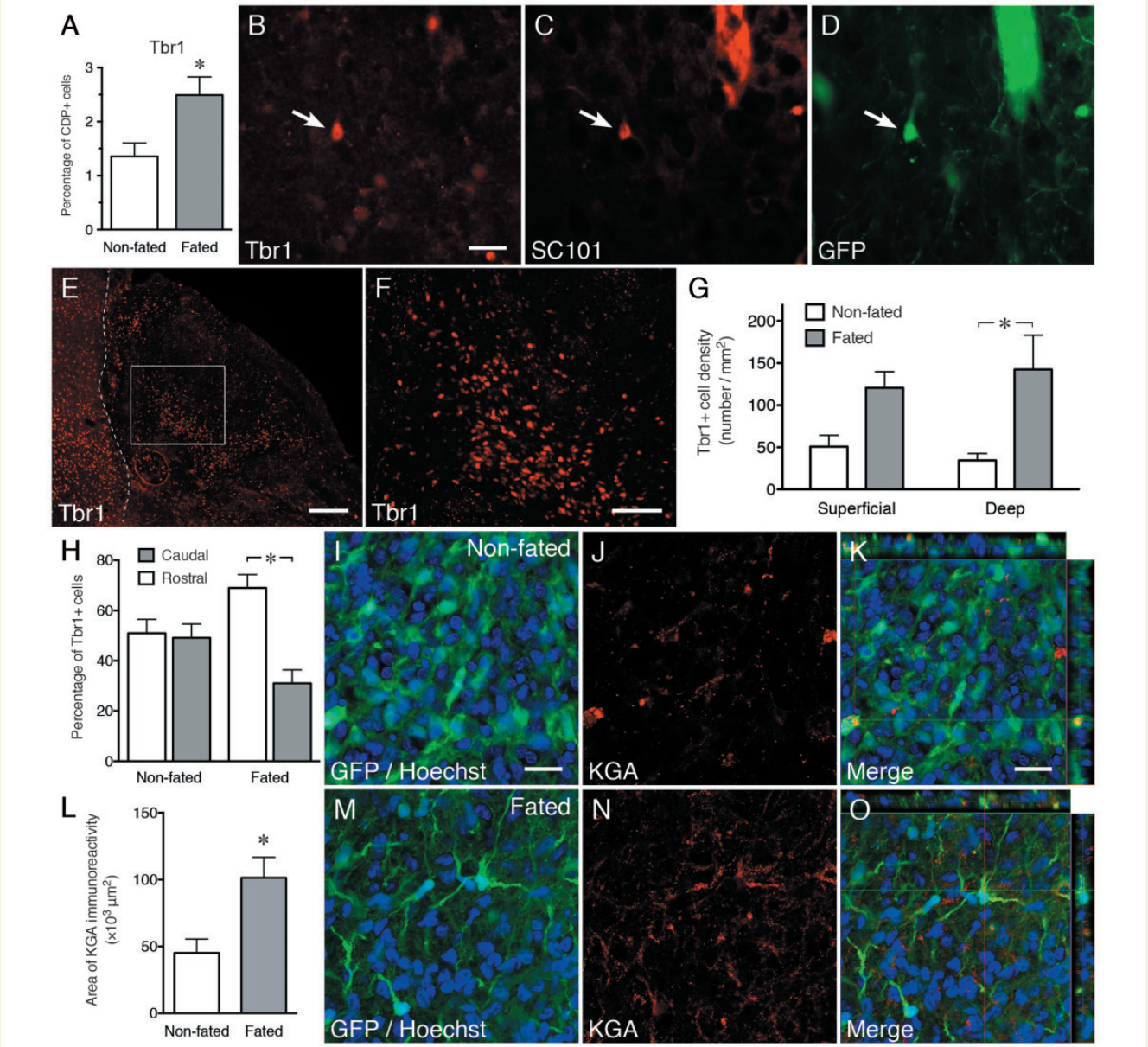

Figure 6 Cortically fated cells differentiate to neurons with cortical phenotype after transplantation in stroke-damaged cortex. (**A**) Quantification of transplanted non-fated and fated human cells immunoreactive for TBR1 in the graft expressed as percentage of SC101 + cells. Mean ± SEM. $*P < 0.05$, Student's unpaired *t*-test. (**B–D**) Representative images of cortically grafted cell (arrows) immunoreactive for TBR1 and showing pyramidal morphology. (**E** and **F**) Preferential localization of TBR1 + cells to deeper layers in grafts with fated cells. Dashed line represents the border between the host cortex (*left*) and the graft (*right*). Area in the square is shown at higher magnification in **F**. (**G**) Quantification of density of TBR1 + cells in superficial and deep areas of grafts of non-fated and fated cells. (**G**) Quantification of percentage of TBR1 + cells in rostral and caudal areas of grafts of non-fated and fated cells. For **G** and **H** means ± SEM. $*P < 0.05$, Student's unpaired *t*-test. (**I–O**) Immunoreactivity for kidney-type glutaminase (KGA) of grafts of non-fated and fated cells. Confocal photomicrographs of representative images of grafts with non-fated (**I–K**) and fated (**M–O**) cells stained with antibody against kidney-type glutaminase. Average reconstructions with Hoechst (blue) and GFP (green) (**I** and **M**) and kidney-type glutaminase (red, **J** and **N**) and orthogonal view (**K** and **O**). (**L**) Quantification of immunoreactivity. Mean ± SEM. $*P < 0.05$, Student's unpaired *t*-test. Scale bars: **B** = 20 µm also for **C** and **D**; **E** = 250 µm; **F** = 100 µm; **I** = 20 µm also for **J**, **M** and **N**; **K** = 20 µm also for **O**.

functionality and cortical phenotype, and being consistent with previously published data (Kim *et al.*, 2011; Wilcox *et al.*, 2011).

The ischaemic lesion was confined to parietal and frontal cortical areas, mainly affecting somatosensory cortex. We found that transplantation of the human induced PSC-derived long-term expandable NES cells 48 h after distal middle cerebral artery occlusion resulted in a partial regeneration of the stroke cavity through the migration of the grafted cells, probably driven by lesion-induced tropism (Kelly *et al.*, 2004). At 2 months after transplantation, the human induced PSC-derived cells proliferated,

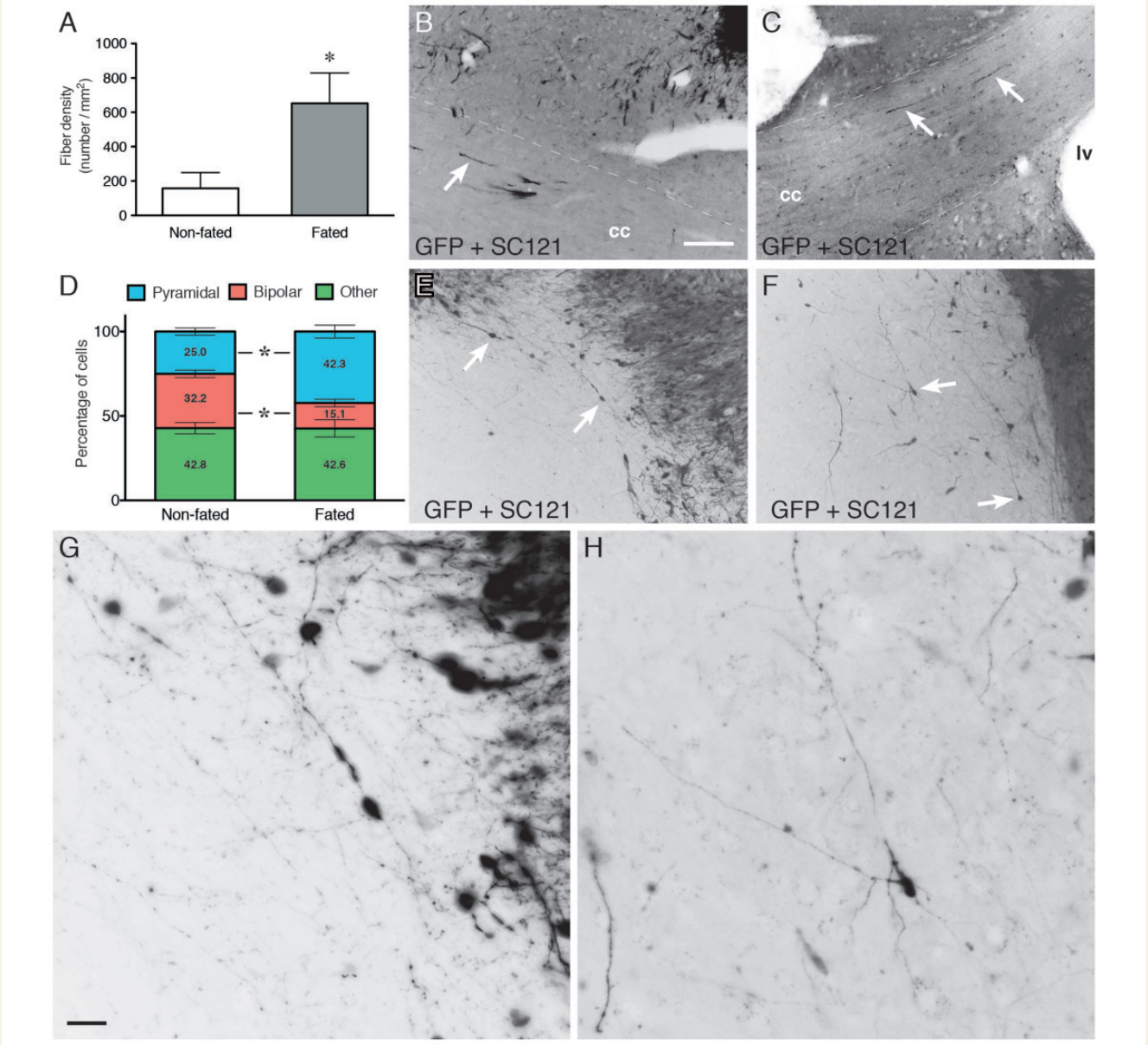

Figure 7 Cortically fated cells transplanted in stroke-damaged cortex exhibit cortical neuronal morphology and generate high projection density in corpus callosum. (**A–C**) Stereological quantification (**A**) and two representative images of GFP and SC121+ fibres (black) from different areas of the corpus callosum in a fated cell-transplanted animal (**B** and **C**). Means ± SEM. $*P < 0.05$, Student's unpaired *t*-test. (**D**) Comparison of the percentage of cells with pyramidal-like and bipolar morphology in non-fated and fated grafts. $*P < 0.05$, two-way ANOVA. (**E–H**) Cells, stained with GFP and SC121 (black), with bipolar morphology are more frequent in non-fated cell grafts (**E**; arrows, the lower one showed with higher magnification in **G**) whereas pyramidal-like morphology is preferentially found in cortically fated grafts (**F**; arrows, the upper one showed with higher magnification in **H**). Scale bars: **B** = 100 μm also for **C**, **E** and **F**; **G** = 20 μm also for **H**. cc = corpus callosum; lv = lateral ventricle.

survived and had generated mature neurons maintaining the cortical phenotype observed *in vitro*. The fated cells exhibited more pyramidal cell-like morphology and projection density in the corpus callosum, and grafts of these cells gave rise to higher percentage of neurons expressing the cortex-specific marker TBR1 as well as better restitution of the cortical layered pattern. The area of immunoreactivity for the glutamatergic neuron-specific marker kidney-type glutaminase was also larger in the grafts of fated cells as compared to the non-fated ones at 2 months after transplantation. The development of projections from the grafted cells and in particular the fated ones provided further evidence of their integration in the host brain. In analogy to our findings, transplantation of murine embryonic stem cell-derived neuroprecursors generated by co-culture with the MS5 stromal line (Ideguchi *et al.*, 2010) and human embryonic stem cell-derived cortical precursors obtained using differentiation defined medium

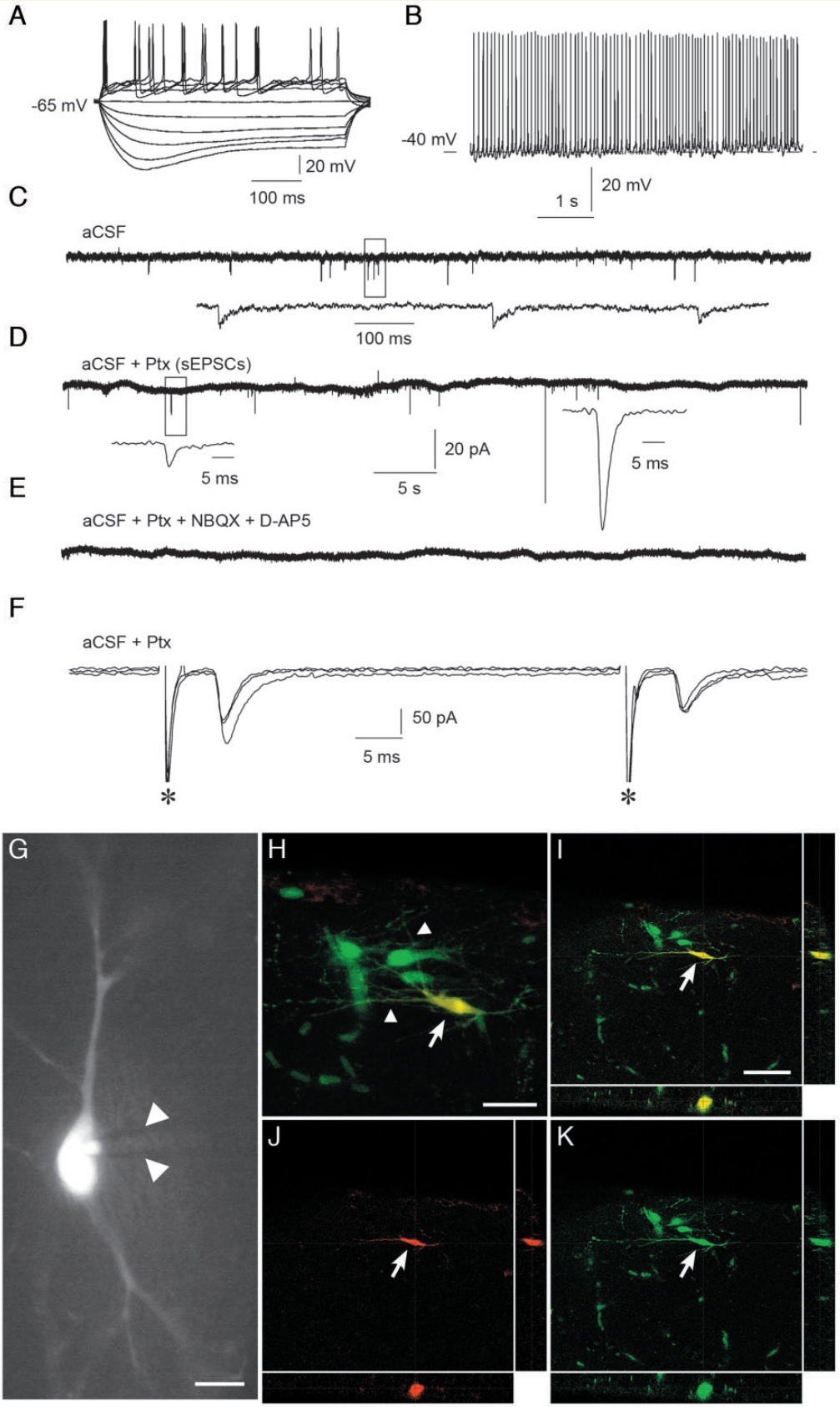

Figure 8 Human induced pluripotent stem-derived cells grafted into the stroke-damaged cortex display electrophysiological properties of mature functional neurons at 5 to 6 months after transplantation into stroke-damaged cortex. (**A**) Representative traces of membrane potential responses elicited by delivering depolarizing and hyperpolarizing current in 10 pA steps. (**B**) Representative trace of spontaneous

(continued)

supplemented with B27 and Noggin (Espuny-Camacho *et al.*, 2013) into the cortex of intact neonatal mice gave rise to pyramidal neurons with similar characteristics.

The electrophysiological data from brain slices containing grafted cells showed that they had differentiated to functional neurons 5 months after transplantation in stroke-damaged cortex. The cells had acquired mature electrical properties, being able to fire action potentials. Integration of these cells into host circuitry was supported by the occurrence of spontaneous and evoked responses. This was observed also in the presence of a GABA receptor antagonist but disappeared in the presence of NBQX and D-AP5, providing evidence of glutamatergic afferents. Previous studies have shown that embryonic stem cell-derived cells transplanted into stroke-damaged brain can generate cells with electrophysiological properties of mature neurons and receive synaptic inputs (Buhnemann *et al.*, 2006; Daadi *et al.*, 2009). We recently showed that non-fated human induced PSC-derived long-term expandable NES cells transplanted into intact rat striatum and cortex can develop excitatory synaptic imputs and functionally integrate, at least in part, into host neural circuitry (Oki *et al.*, 2012). Here we did not find any significant differences between non-fated and fated cells 5 months after transplantation. Analysis at later time points will likely be necessary to distinguish subtle differences associated with the further maturation of the human-derived fated cells.

The behavioural tests revealed deficits in sensorimotor function at 1 week after the cortical stroke. We speculate that the rapidly observable impairment of the contralateral forelimb in the forehand direction of the stepping test could be caused by the acute loss of neurons in the ischaemic lesion, whereas the slower development of pathology in adjusting steps for the ipsilateral forelimb might reflect secondary degeneration of neurons in connected contralateral cortical areas. Interestingly, the cell-transplanted groups showed improved performance in adjusting steps of both forelimbs at 8 weeks. Here we did not aim to identify the mechanisms underlying the improvements induced by the cortically fated cells at different time points after transplantation. However, it is unlikely that neuronal replacement and reconstruction of circuitry by the human induced PSC-derived long-term expandable NES cells is the major mechanism underlying the improvement at 8 weeks. Conceivably, though, functional integration of the grafted mature neurons, probably occurring several months later, would lead to further improvement. Longer observation times are required to assess whether functional integration of the grafted mature neurons, which probably occurs several months later, would lead to further improvement. The appearance of the graft-induced behavioural improvement at eight but not at 1 or 4 weeks suggests a mechanism related to alterations of the environment by the new cells, e.g. modulation of the inflammatory processes (Mine *et al.*, 2013). The absence of early functional recovery, as observed in parallel to elevated vascular endothelial growth factor levels at 2 weeks after intrastriatal transplantation of non-fated human induced PSC-derived long-term expandable NES cells in mice subjected to middle cerebral artery occlusion (Oki *et al.*, 2012), argues against a significant role of vascular endothelial growth factor in the graft effect seen here. Being consistent with the bilateral recovery in the stepping test, the ipsi- and contralateral projections of the grafted cells and the afferents they receive could contribute to recovery by counteracting the secondary degeneration in different areas of the host brain (Polentes *et al.*, 2012). Various mechanisms have been implicated in this process (Bacigaluppi *et al.*, 2009), but cell therapy seems to

Table 3 Electrophysiological properties of transplanted non-fated and fated cells generating one or more action potentials upon current injections

	Non-fated	Fated
n	6	4
V_{rest} (mV)	−52.1 ± 6.6	−50.8 ± 5.7
R_{input} (MΩ)	1590 ± 431	1214 ± 290
C (pF)	20.9 ± 7.1	8.8 ± 1.4

V_{rest} = resting membrane potential; R_{input} = input resistance; C = capacitance.
No significant differences were detected between non-fated and fated cells (unpaired *t*-tests for V_{rest} and R_{input} and unpaired *t*-test with Welch's correction for capacitance).

Table 4 Action potential characteristics for transplanted fated and non-fated cells

	Fated	Non-fated
% cells w. AP (cells w AP/total)	21 (4/19)	35 (6/17)
AP threshold (mV)$	−36.0 ± 1.5	−31.9 ± 1.5
AP amplitude (mV)$	47.8 ± 8.7	48.6 ± 6.2
AP half-height width (ms)$	1.7 ± 0.2	1.3 ± 0.3
AHP amplitude (mV)$	9.9 ± 1.8	13.8 ± 1.1

$Analysis based on the first action potential induced by current injection.
No significant differences were detected between fated and non-fated action potential cells (unpaired *t*-tests).
AP = action potential.

Figure 8 Continued
action potentials observed in current clamp at 0 pA. (**C**) Representative traces of spontaneous postsynaptic currents, and (**D**) spontaneous excitatory postsynaptic currents recorded in the presence of picrotoxin (Ptx), which were blocked by addition of glutamate receptor antagonists, NBQX and D-AP5 (**E**). Insets in **C** and **D** show respective events on an expanded scale. (**F**) Evoked response observed in a cell after electrical stimulation of the cortex distant from the graft site (three responses superimposed, asterisk denotes stimulation artefact). Cells were held at −70 mV during voltage-clamp recordings. (**G**) Photomicrograph of a grafted GFP+ recorded cell with the patch-pipette (arrowheads). (**H–J**) Confocal images of another biocytin-labelled cell (arrows); (**H**) average composition of one recorded cell stained for GFP after recording, note the high number of neurites (arrowhead), (**I–K**) orthogonal views of the same cell as merged (**I**), only byocitin (**J**) and only GFP (**K**) staining. Scale bars: **G** = 25 μm; **H** = 50 μm; **I–K** = 100 μm. aCSF = artificial CSF.

be able to promote the recovery of fast axonal transport disrupted after stroke (Andres *et al*., 2011).

A previous study (Kawai *et al*., 2010) showed that human induced PSCs can exhibit high tumorigenicity after transplantation into the stroke-injured brain. Consistent with our previous findings using human induced PSC-derived long-term expandable NES cells (Oki *et al*., 2012), we did not detect any tumour formation in grafts of either fated or non-fated cells in immunocompromised rats at 5 months following stroke. The cortically fated cells proliferated less than the non-fated ones and similar to the human induced PSC-derived long-term expandable NES cells in the study by Oki *et al.* (2012), and were more efficient in generating mature neurons at 2 months. Moreover, the proliferative activity at 5 months after the insult in the grafts of fated cells was very low (1.6%; unpublished observation), as observed in sections through slices used for electrophysiology. In accordance, Oki *et al*. (2012) found proliferative activity of 1% in human induced PSC-derived long-term expandable NES cell grafts at 4 months after transplantation. Taken together, our data indicate that transplantation of predifferentiated human induced PSC-derived long-term expandable NES cells into the stroke-damaged brain is associated with minimal risk of tumour formation.

The generation of specific subtypes of neurons will be necessary for neuronal replacement-based therapeutic strategies in human neurodegenerative disorders. Human induced PSC-derived dopaminergic neurons have been shown to survive and improve behavioural impairments after intrastriatal transplantation in an animal model of Parkinson's disease (Hargus *et al*., 2010). Here we show, for the first time, that neurons of cortical phenotype can be generated from human induced PSCs, and survive, integrate and function after intracortical implantation in a clinically relevant animal model of stroke. Further studies will be needed to clarify in detail the mechanisms of action of these cortical neurons and their capacity to induce behavioural improvements by replacing those cortical neurons, which have died after the insult. Although our findings only represent a very early step, they bring closer the clinical translation of human induced PSCs for neuronal replacement by autologous transplantation in stroke patients.

Acknowledgements

We thank Camilla Ekenstierna for technical assistance.

Funding

This work was supported by grants from Swedish Research Council, European Union project TargetBraIn (279017), AFA Foundation, Swedish Government Initiative for Strategic Research Areas (StemTherapy), BMBF grant 01GN0813, DFG grant SFB-TR3 D2 and the Hertie Foundation. D.T. was partially supported by grant from Instituto de Salud Carlos III (Spain).

Supplementary material

Supplementary material is available at *Brain* online.

References

Andersson T, Duckworth JK, Fritz N, Lewicka M, Sodersten E, Uhlen P, et al. Noggin and Wnt3a enable BMP4-dependent differentiation of telencephalic stem cells into GluR-agonist responsive neurons. Mol Cell Neurosci 2011; 47: 10–8.

Andres RH, Horie N, Slikker W, Keren-Gill H, Zhan K, Sun G, et al. Human neural stem cells enhance structural plasticity and axonal transport in the ischaemic brain. Brain 2011; 134 (Pt 6): 1777–89.

Bacigaluppi M, Pluchino S, Peruzzotti-Jametti L, Kilic E, Kilic U, Salani G, et al. Delayed post-ischaemic neuroprotection following systemic neural stem cell transplantation involves multiple mechanisms. Brain 2009; 132 (Pt 8): 2239–51.

Buhnemann C, Scholz A, Bernreuther C, Malik CY, Braun H, Schachner M, et al. Neuronal differentiation of transplanted embryonic stem cell-derived precursors in stroke lesions of adult rats. Brain 2006; 129 (Pt 12): 3238–48.

Chang DJ, Lee N, Park IH, Choi C, Jeon I, Kwon J, et al. Therapeutic potential of human induced pluripotent stem cells in experimental stroke. Cell Transplant 2012; 22: 1427–40.

Chen SJ, Chang CM, Tsai SK, Chang YL, Chou SJ, Huang SS, et al. Functional improvement of focal cerebral ischemia injury by subdural transplantation of induced pluripotent stem cells with fibrin glue. Stem Cells Dev 2010; 19: 1757–67.

Chen ST, Hsu CY, Hogan EL, Maricq H, Balentine JD. A model of focal ischemic stroke in the rat: reproducible extensive cortical infarction. Stroke 1986; 17: 738–43.

Daadi MM, Davis AS, Arac A, Li Z, Maag AL, Bhatnagar R, et al. Human neural stem cell grafts modify microglial response and enhance axonal sprouting in neonatal hypoxic-ischemic brain injury. Stroke 2010; 41: 516–23.

Daadi MM, Lee SH, Arac A, Grueter BA, Bhatnagar R, Maag AL, et al. Functional engraftment of the medial ganglionic eminence cells in experimental stroke model. Cell Transplant 2009; 18: 815–26.

Darsalia V, Kallur T, Kokaia Z. Survival, migration and neuronal differentiation of human fetal striatal and cortical neural stem cells grafted in stroke-damaged rat striatum. Eur J Neurosci 2007; 26: 605–14.

Delavaran H, Sjunnesson H, Arvidsson A, Lindvall O, Norrving B, van Westen D, et al. Proximity of brain infarcts to regions of endogenous neurogenesis and involvement of striatum in ischaemic stroke. Eur J Neurol 2013; 20: 473–9.

Espuny-Camacho I, Michelsen KA, Gall D, Linaro D, Hasche A, Bonnefont J, et al. Pyramidal neurons derived from human pluripotent stem cells integrate efficiently into mouse brain circuits *in vivo*. Neuron 2013; 77: 440–56.

Falk A, Koch P, Kesavan J, Takashima Y, Ladewig J, Alexander M, et al. Capture of neuroepithelial-like stem cells from pluripotent stem cells provides a versatile system for *in vitro* production of human neurons. PLoS One 2012; 7: e29597.

Gaspard N, Bouschet T, Herpoel A, Naeije G, van den Ameele J, Vanderhaeghen P. Generation of cortical neurons from mouse embryonic stem cells. Nat Protoc 2009; 4: 1454–63.

Gaspard N, Bouschet T, Hourez R, Dimidschstein J, Naeije G, van den Ameele J, et al. An intrinsic mechanism of corticogenesis from embryonic stem cells. Nature 2008; 455: 351–7.

Gomi M, Takagi Y, Morizane A, Doi D, Nishimura M, Miyamoto S, et al. Functional recovery of the murine brain ischemia model using human induced pluripotent stem cell-derived telencephalic progenitors. Brain Res 2012; 1459: 52–60.

Hand R, Bortone D, Mattar P, Nguyen L, Heng JI, Guerrier S, et al. Phosphorylation of Neurogenin2 specifies the migration properties and the dendritic morphology of pyramidal neurons in the neocortex. Neuron 2005; 48: 45–62.

Hansen DV, Rubenstein JL, Kriegstein AR. Deriving excitatory neurons of the neocortex from pluripotent stem cells. Neuron 2011; 70: 645–60.

Hargus G, Cooper O, Deleidi M, Levy A, Lee K, Marlow E, et al. Differentiated Parkinson patient-derived induced pluripotent stem

cells grow in the adult rodent brain and reduce motor asymmetry in Parkinsonian rats. Proc Natl Acad Sci USA 2010; 107: 15921–6.

Hebert JM, Mishina Y, McConnell SK. BMP signaling is required locally to pattern the dorsal telencephalic midline. Neuron 2002; 35: 1029–41.

Hicks AU, Lappalainen RS, Narkilahti S, Suuronen R, Corbett D, Sivenius J, et al. Transplantation of human embryonic stem cell-derived neural precursor cells and enriched environment after cortical stroke in rats: cell survival and functional recovery. Eur J Neurosci 2009; 29: 562–74.

Ideguchi M, Palmer TD, Recht LD, Weimann JM. Murine embryonic stem cell-derived pyramidal neurons integrate into the cerebral cortex and appropriately project axons to subcortical targets. J Neurosci 2010; 30: 894–904.

Jiang M, Lv L, Ji H, Yang X, Zhu W, Cai L, et al. Induction of pluripotent stem cells transplantation therapy for ischemic stroke. Mol Cell Biochem 2011; 354: 67–75.

Kawai H, Yamashita T, Ohta Y, Deguchi K, Nagotani S, Zhang X, et al. Tridermal tumorigenesis of induced pluripotent stem cells transplanted in ischemic brain. J Cereb Blood Flow Metab 2010; 30: 1487–93.

Kelly S, Bliss TM, Shah AK, Sun GH, Ma M, Foo WC, et al. Transplanted human fetal neural stem cells survive, migrate, and differentiate in ischemic rat cerebral cortex. Proc Natl Acad Sci USA 2004; 101: 11839–44.

Kim DS, Lee JS, Leem JW, Huh YJ, Kim JY, Kim HS, et al. Robust enhancement of neural differentiation from human ES and iPS cells regardless of their innate difference in differentiation propensity. Stem Cell Rev 2010; 6: 270–81.

Kim JE, O'Sullivan ML, Sanchez CA, Hwang M, Israel MA, Brennand K, et al. Investigating synapse formation and function using human pluripotent stem cell-derived neurons. Proc Natl Acad Sci USA 2011; 108: 3005–10.

Koch P, Opitz T, Steinbeck JA, Ladewig J, Brustle O. A rosette-type, self-renewing human ES cell-derived neural stem cell with potential for *in vitro* instruction and synaptic integration. Proc Natl Acad Sci USA 2009; 106: 3225–30.

Kuwabara T, Hsieh J, Muotri A, Yeo G, Warashina M, Lie DC, et al. Wnt-mediated activation of NeuroD1 and retro-elements during adult neurogenesis. Nat Neurosci 2009; 12: 1097–105.

Larsen JO, Gundersen HJ, Nielsen J. Global spatial sampling with isotropic virtual planes: estimators of length density and total length in thick, arbitrarily orientated sections. J Microsc 1998; 191: 238–48.

Li XJ, Zhang X, Johnson MA, Wang ZB, Lavaute T, Zhang SC. Coordination of sonic hedgehog and Wnt signaling determines ventral and dorsal telencephalic neuron types from human embryonic stem cells. Development 2009; 136: 4055–63.

Lindvall O, Kokaia Z. Stem cell research in stroke: how far from the clinic? Stroke 2011; 42: 2369–75.

Mariani J, Simonini MV, Palejev D, Tomasini L, Coppola G, Szekely AM, et al. Modeling human cortical development *in vitro* using induced pluripotent stem cells. Proc Natl Acad Sci USA 2012; 109: 12770–5.

Mine Y, Tatarishvili J, Oki K, Monni E, Kokaia Z, Lindvall O. Grafted human neural stem cells enhance several steps of endogenous neurogenesis and improve behavioral recovery after middle cerebral artery occlusion in rats. Neurobiol Dis 2013; 52: 191–203.

Oki K, Tatarishvili J, Wood J, Koch P, Wattananit S, Mine Y, et al. Human-induced pluripotent stem cells form functional neurons and improve recovery after grafting in stroke-damaged brain. Stem Cells 2012; 30: 1120–33.

Olsson M, Nikkhah G, Bentlage C, Bjorklund A. Forelimb akinesia in the rat Parkinson model: differential effects of dopamine agonists and nigral transplants as assessed by a new stepping test. J Neurosci 1995; 15 (5 Pt 2): 3863–75.

Polentes J, Jendelova P, Cailleret M, Braun H, Romanyuk N, Tropel P, et al. Human induced pluripotent stem cells improve stroke outcome and reduce secondary degeneration in the recipient brain. Cell Transplant 2012; 21: 2587–602.

Shi Y, Kirwan P, Smith J, Robinson HP, Livesey FJ. Human cerebral cortex development from pluripotent stem cells to functional excitatory synapses. Nat Neurosci 2012; 15: 477–86.

Shimogori T, Banuchi V, Ng HY, Strauss JB, Grove EA. Embryonic signaling centers expressing BMP, WNT and FGF proteins interact to pattern the cerebral cortex. Development 2004; 131: 5639–47.

Shoemaker LD, Arlotta P. Untangling the cortex: advances in understanding specification and differentiation of corticospinal motor neurons. Bioessays 2010; 32: 197–206.

Wilcox JT, Lai JK, Semple E, Brisson BA, Gartley C, Armstrong JN, et al. Synaptically-competent neurons derived from canine embryonic stem cells by lineage selection with EGF and Noggin. PLoS One 2011; 6: e19768.